한국표면공학회지
Journal of the Korean Institute of Surface Engineering
Vol. 33, No. 4, Aug. 2000
<연구논문>

Determination of the Failure Paths of Leadframe/EMC Joints

H. Y. Lee* and S. R. Kim**

*Dept. of Materials Science and Engineering, Korea Advanced Institute of Science and Technology, 373-1 Kusong-dong, Yusong-gu, Taejon 305-701, KOREA
**Senior Scientist Polymeric Materials Gr., Sam Yang Central R&D Center, 63-2 Hwaam-dong, Yusong-gu, Taejon, 305-348 KOREA

Abstract

Popcorn cracking phenomena frequently occur in thin plastic packages during the solder reflow process, which are definitely affected by poor adhesion of Cu-based leadframe to epoxy molding compounds (EMCs). In the present work, in order to enhance the adhesion strength, a brown-oxide treatment on the Cu-based leadframe was carried out and the adhesion strength of leadframe/EMC interface was measured in terms of fracture toughness by using sandwiched double-cantilever beam (SDCB) specimens. After the adhesion tests, fracture surfaces were analyzed by SEM, AES, EDS and AFM to make the failure path clear. Results showed that failure path was closely related to the oxidation time and the interfacial fracture toughness.

1. INTRODUCTION

Thin plastic packages of surface mounting type are widely used in packaging industry because they satisfy the requirement for getting more function in a smaller electronic device[1]. However, as the package thickness becomes thinner, moisture-related problems such as popcorn cracking phenomena increase, especially for the packages with larger die or pad sizes[2-5]. Popcorn cracks generated during the solder reflow process due to the combination of vapor pressure exerting on the delaminated region and thermal stress resulted from the mismatch of coefficient of thermal expansion (CTE) among package components[6-8].

Due to their higher electrical and thermal property as well as higher reliability of solder joint compared with Alloy-42 leadframe, copper-based alloy leadframes are being widely used[9]. However, lower adhesion strength of Cu-based leadframe to EMC than that of alloy 42 leadframe, the occurrence of package delamination or cracking with copper-based alloy leadframe is said to be higher compared with alloy 42 leadframe. Such a poor nature of adhesion can be strengthened by using various surface treatment techniques[6,7,10-14].

In this work, the adhesion strength of Cu-based leadframe/EMC interface was varied by

forming of brown-oxide layer on the leadframe surface before molding with EMC, and the adhesion strength of leadframe/EMC interface was measured in terms of fracture toughness by using sandwiched double-cantilever beam (SDCB) specimens. In addition, fracture surfaces were analyzed by SEM, AES, EDS and AFM to make the failure path clear.

2. EXPERIMENTAL PROCEDURE

2. 1. Formation of Brown Oxide

Copper-based leadframes (commercial name : EFTEC-64T) with the nominal composition of Cu-0.3Cr-0.25Sn-0.2Zn and thickness of 0.15 mm were used. Organic impurities on the leadframe surfaces were removed by ultrasonic cleaning in acetone for 20 minutes and subsequently native oxides were removed by pre-treatment solution (commercial name : Activan #6, a brand of Han Yang Chemical Ind., Korea). After the pre-conditioning, leadframe sheets were immersed in the hot alkaline solution to form a brown-oxide layer on the surface[13]. The oxidation times were less than 20 minutes. The brown-oxide layer was analyzed by SEM, TEM and glancing-angle X-ray diffractometer (XRD). Then, the oxide thickness was measured by the galvanostatic reduction method[15-17], which is described minutely in the reference[15].

2. 2. Preparation of SDCB Specimens and Mechanical Tests

After the surface modification, leadframe sheets were compounded with EMC (oxygen-carbon-nitrogen type, DMC-20 by Dong-Jin Chemical Co., Korea) in a compression molding system for 15 minutes at 175℃ and then machined into SDCB specimens for the fracture toughness testing[18]. After the machining, all specimens were post-cured at 175℃ for 4 hours. The fracture toughness or critical energy-release rate, G_{IC} was calculated from equation (1) on the basis of the reference[19] ;

$$G_{IC}=\frac{P_C^2 a^2}{t^2 l^3 \overline{E}}\left[3.467+2.315\left(\frac{l}{a}\right)\right]^2 \qquad (1)$$

where, P_C is the critical load, $\overline{E}$ is the plane strain tensile modulus defined by $E/(1-\nu^2)$ (E : Young's modulus, ν : Poisson's ratio), a is the crack length, t is the sepcimen thickness, and l is the specimen half-height, respectively. A sandwiched specimen can be regarded as a homogeneous specimen when the inserted layer is sufficiently small compared to the other specimen geometry[20].

3. RESULTS AND DISCUSSION

3. 1. Oxidation Characteristics

Scanning electron micrographs of leadframe samples oxidized in the brown-oxide forming solution were presented in the reference[18]. Fine acicular oxide precipitates typically 100~300 nm in length covered the entire area of surface after 1 or 2 minutes. With subsequent X-ray and galvanostatic reduction analyses, the fine acicular precipitates were later proved to be CuO[18]. With all the further oxidation time, the size and density of the oxide precipitates only increased slightly, and remained more or less the same after 2 minutes. According to the thickness

measurements, the average thickness of CuO layer reached around 150 nm after 1.5 minutes of the oxidation time[18]. There was no change in thickness with further oxidation time, which was consistent with the results from SEM and X-ray analyses.

3. 2. Fracture Toughness

The fracture toughness of the leadframe/EMC interface was measured in terms of the critical energy-release rate, G_{IC} by using SDCB specimens and the results were presented in the reference[18]. The fracture toughness was nearly zero for the untreated leadframe but increased almost linearly with the oxidation time up to 1 minute and reached the saturation value of around 80 J/m^2 at 2 minutes. It appeared that the change of G_{IC} was similar to the thickening kinetics of CuO.

3. 3. Fracture Surface Analyses

3. 3. 1 SEM Analyses

Fracture surfaces were photographed in a secondary electron microscope, and the results are presented in Fig. 1. Comparing between micrographs taken from the separated leadframe side and EMC side, it can be stated that fractography was changed with the oxidation time ; in the early stage of oxidation, non-dimple type (A-type) failure occurred, but when the oxidation time was more than 2 minutes, dimple type (B-type) failure took place.

For A-type specimens, clod-like debris with black color are seen from the separated leadframe sides (Fig. 1 (a), (c)), and their counterpart, separated EMC sides (Fig. 1 (b), (d)), were observed to be torn away severely. It is well known fact that light and darkness in SEM micrographs closely related to the emission rate of secondary electron ; the higher emission rate of secondary electron, the lighter images are acquired. The formulation for most EMCs consist of a complicated and often proprietary mixture of epoxy resin, hardener(or curing agent), catalyst(s), fillers, flame retardents, flexibilizers, coupling agents, mold release agents, and colorants. The EMC used in this experiment consists of epoxy resin of OCN(oxygen-carbon-nitrogen) type and some additives. The epoxy resin and CuO are known as nonconducting and p-type semiconducting substances[21], respectively. The contrast between light and darkness in SEM micrographs may be due to the electronic properties of epoxy resin and CuO. Generally, the emission rate of secondary electron is higher for the semiconducting materials than for the nonconducting materials[22, 23]. Considering leadframe and EMC were adhered together before mechanical testing and epoxy resin is relatively weak, the clod-like debris with black color on the separated leadframe sides are presumed to be EMC clumps.

3. 3. 2 AES analyses

To confirm the above inference, AES survey analyses on the selected two regions of the separated leadframe side of A-type specimen was carried out and the results are presented in Fig. 2. Since the carbon element can be introduced on the surface by contamination, it is necessary to confirm it is from surface contamination or not by Ar ion etching for 0.2 min. As expected previously, the large amount of carbon and oxygen elements were detected on the surface of

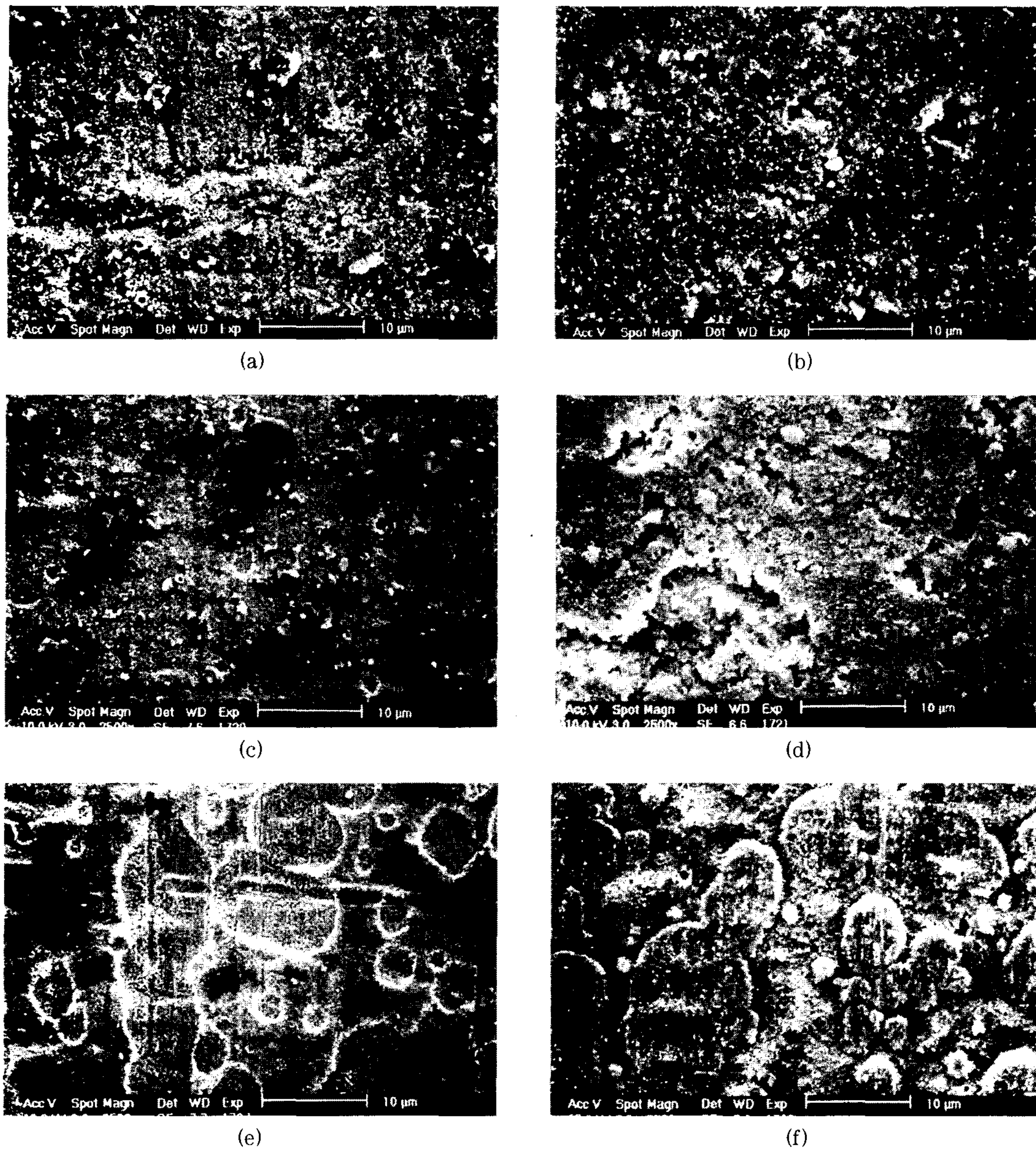

Fig. 1. SEM micrographs out of leadframe side and EMC side. (a), (c) and (e) are leadframe sides of the oxidation times of leadframe before molding are 30 seconds, 1 minute and 2 minutes, respectively. (b), (d) and (f) are EMC sides of the (a), (c) and (e), respectively.

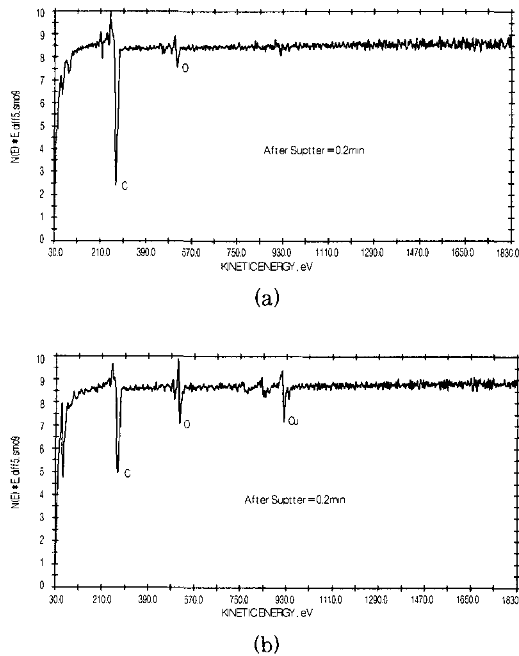

Fig. 2. AES survey of (a) clod-like debris region and (b) non-debris region.

clod-like debris even after 0.2 min Ar ion etching. From this result it might be stated that the carbon element detected here are evidently presumed to be from epoxy resin. This indicates the cohesive failure of EMC predominantly occurred in the debris region.

On the other hand, three elements (carbon, oxygen and copper) were detected in the non-debris region, and such result might be attributable to the failure occurrence in the vicinity of the CuO/EMC interface. Since CuO crystals have a needle shape, they interlock into EMC so that the roughness of CuO/EMC interface must be very high. Thus, in case of the occurrence of crack propagation along CuO/EMC interface, a lot of carbon certainly comes to remain on the separated leadframe side.

For B-type specimens, cohesive failure was very likely to happen, because the dimple-shaped morphologies are seen from both SEM micrographs taken from the separated leadframe side (Fig. 1 (e)) and its corresponding separated EMC side (Fig. 1 (f)). To get more information about fracture surface, AES survey analyses were also carried out on the selected two regions of the separated leadframe side, convex region and concave region. The results are presented in Fig. 3. It is shown that in spite of the Ar etching for 0.2 min, the carbon element was still detected, and also oxygen and copper elements were detected in the convex region. The amount of carbon in the convex region was much more than that in the concave region. This indicates that carbon element in the convex region evidently came from EMC and oxygen and copper el-

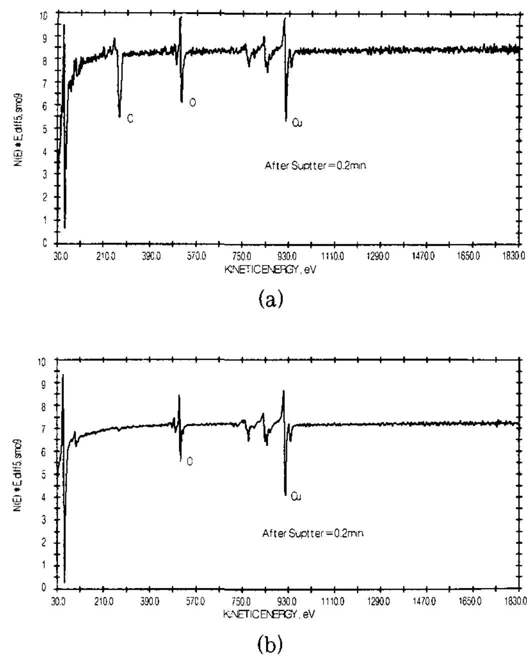

Fig. 3. AES survey of (a) convex region and (b) concave region of separated leadframe side of which the oxidation time is two minutes.

ements came from CuO. With above results and the characteristic of CuO/EMC interface, it can be said that fracture occurred in the vicinity of CuO/EMC interface in the convex region.

On the other hand, the concave region contains much less carbon elements than the convex region does and almost the same copper and oxygen elements. Taking it into consideration that the detection of oxygen and copper elements in the concave region and the constitution of brown-oxide (CuO), it strikes that failure might occur in the inside of the CuO on the concave region.

3. 3. 3 EDS analyses

To confirm the previously mentioned failure path, analyses on the copper distribution (Cu mapping) were conducted in the separated EMC side by using EDS (electron dispersive spectroscopy). Note that the mapping information acquired by using EDS gives only quantitative information about specific element. The Cu mapping result is shown in Fig. 4. There is a lot of copper element in the convex region but the opposite is true for the concave region. Recalling that EMC inherently does not contain copper element and the counter part of the convex region of the separated EMC side is the concave region of the separated leadframe side, EDS result supports the previous inference on the failure path of the B-type specimens.

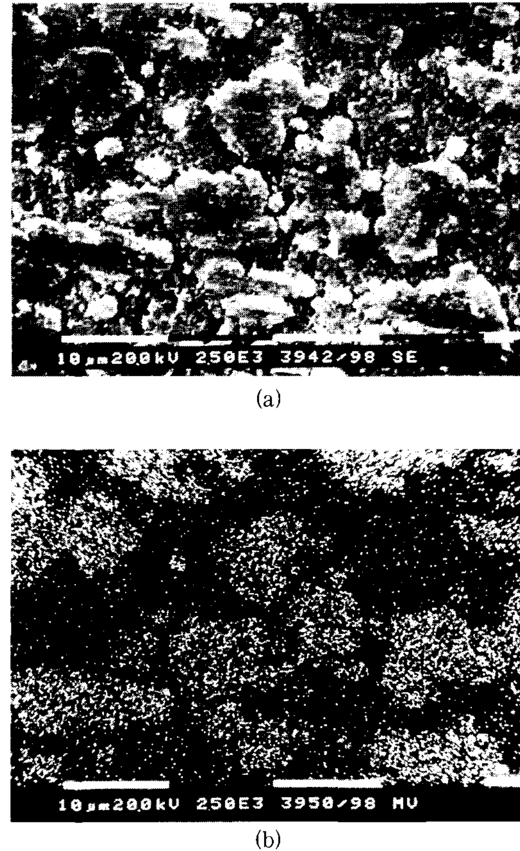

(a)

(b)

Fig. 4. SEM micrograph and its corresponding copper-mapping image out of EMC side separated from four-minute-oxidized leadframe.

3. 3. 4 AFM and TEM analyses

AFM analyses on the fracture surface carried out to know the height difference between convex and concave region. 10μm×10μm area was scanned. Acquired images and line profiles are shown in Fig. 5. According to the line profile results, the height differences in leadframe side and EMC side were 316.1 nm and 440 nm, respectively.

The cross-sectional TEM image was taken from the twenty-minute-oxidized leadframe sheet and shown in Fig. 6. The CuO needles and the gaps among the CuO needles are found. The real length of CuO needles is estimated at more than 0.5μm on the basis of this TEM micrograph. Comparing between the average thickness of CuO layer measured by galvanostatic reduction method, 0.15μm, and the real length of CuO nee-

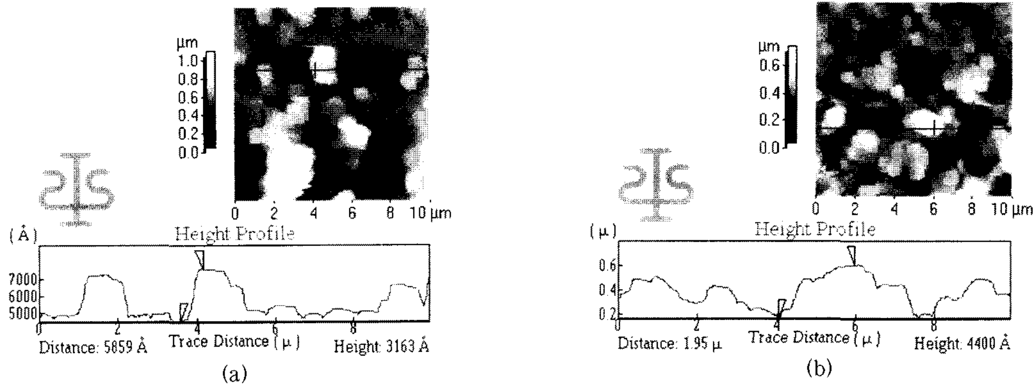

Fig. 5. AFM images and line profiles on the (a) leadframe side and (b) EMC side separated from four-minute oxidized leadframe.

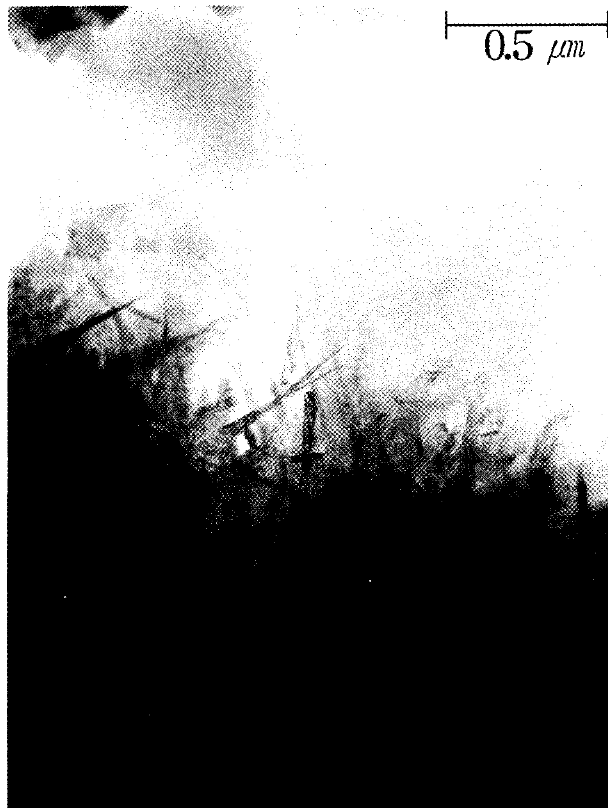

Fig. 6. Cross-sectional TEM micrograph of twenty-minute-oxidized leadframe.

dle, $0.5 \sim 0.8 \mu m$, it becomes clear that most part of CuO layer is filled with voids or gaps. Such voids or gaps may play an important role in the penetration of epoxy resin, that is why the mechanical interlocking is achieved between CuO needles and epoxy resin during the molding

process.

Considering the real length of CuO needles, the line profile results are quite coincident with the previous AES results, of Fig. 3.

3. 3. 5 Failure paths

Previous analyses on the fracture surface by using SEM, AES, EDS and AFM showed that failure occurred in a mixed mode for both A-type and B-type specimens. When the oxidation time is below two minutes (A-type specimens), failure occurred in a nearly interfacial mode near by the CuO/EMC interface in the non-debris region of the separated leadframe side and in a cohesive mode in the inside of EMC in the debris region. On the other side, when the oxidation time is more than two minutes (B-type specimens), nearly interfacial failure occurred in the vicinity of CuO/EMC interface, and cohesive failure in the inside of the CuO occurred in the convex region and concave region of the separated leadframe side, respectively. Schematic diagrams delineating the failure paths are shown in Fig. 7.

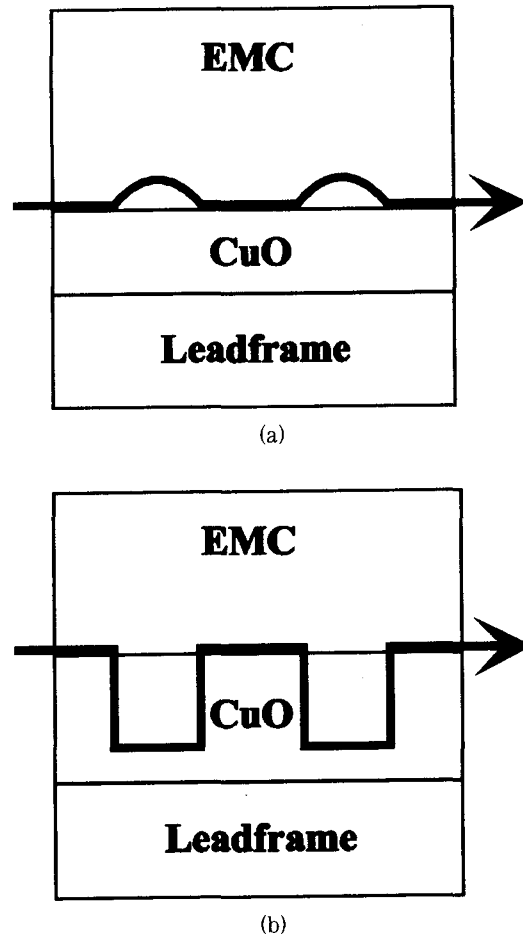

Fig. 7. Schematic illustrations of failure paths : (a) is for low oxidation time ($t<2$ minutes) and (b) is for high oxidation time ($t\geq2$ minutes)

The reason why the nearly interfacial failure occurred may be ascribed to the real length of CuO needles. In case of the early stage of oxidation (A-type specimens), since the real length of CuO needles is short, the penetrating depth of epoxy resin into gaps among CuO needls must be short. Consequently, the mechanical interlocking between CuO needls and EMC is so weak that the fracture toughness of CuO/EMC interface is also weak. Hence most of failure occurs near by CuO/EMC interface with some exception. However, in case of the oxidation time is more than two minutes (B-type specimens), the entire area of leadframe is already covered with fully-grown CuO needls so that the penetrating depth of epoxy resin is saturated. Such a saturated penetrating depth may affect on the interfacial fracture toughness and fracture behavior. Recalling that the variation of G_{IC} with the oxidation time and the fracture behavior, it might be said that fracture toughness and failure behavior are closely related to the failure paths for the brown-oxide and EMC system.

4. CONCLUSIONS

1) Brown-oxide treatment of Cu-based leadframe introduced fine acicular CuO precipitates on the surface and the average thickness of CuO layer increases up to around 150 nm within 2 minutes of the oxidation time.

2) The interfacial fracture toughness increased almost proportionally with the thickness of CuO layer and reached a saturation value of around 80 J/m^2 at two minutes of the oxidation time.

3) Fine acicular CuO precipitates contributed to the increase of fracture toughness of leadframe/EMC interface by mechanical interlocking with EMC, while untreated smooth surface played no role.

4) From the systematic analyses on the fracture surface, the failure paths were cleared ; when the oxidation time was less than two minutes, failure path lay over near the CuO/EMC interface and in the inside of EMC. However, when the oxidation time is two or more minutes, failure path lay in the vicinity of the CuO/EMC interface and in the inside of CuO.

REFERENCES

1. T. Hannibal and A. Singer : Proc. 48th Electronic Components and Technology Conf., (1998) 471
2. G. S. Ganesan and H. M. Berg : IEEE Trans. on Components, Hybrids, and Manufacturing Technology, 16 (1993) 940
3. M. Adachi. S. Ohuchi and N. Totsuka : IEEE Trans. on Components, Hybrids, and Manufacturing Technology, 16 (1993) 550
4. O. Tay, G. L. Tan, and T. B. Lim : IEEE Trans. on Components, Packaging, and Manufacturing Technology-Part B : Advanced Packaging, 17 (1994) 201
5. J. Sauber, L. Lee, S. Hsu and T. Hongsmatip : IEEE Trans. on Components, Packaging, and Manufacturing Technology - Part A, 17 (1994) 533
6. Lee, W. H sler, H. Cerva, R. von Criegern and A. Parthasarathi : Proc. 48th Electronic Components and Technology Conf., (1998) 1154
7. Q. Cui, H. L. Tay, T. C. Chai, R. Gopalakrishan and T. B. Lim : Proc. 48th Electronic Components and Technology Conf., (1998) 1162
8. A. O. Tay and T. Y. Lin : Proc. 48th Electronic Components and Technology Conf., (1998) 371
9. Y. Tomioka and J. Miyake : 49th Electronic Components and Technology Conf., (1999) 714
10. O. Yoshika, N. Okabe, S. Nagayama, R. Yamagishi and G. Murakami : 39th Electronic Components and Technology Conf., (1989) 464
11. G. Xue, G. Shi, J. Ding, W. Chang and R. Chen : J. Adhesion Sci. Technol., 4 (1990) 723
12. F. Djennas, E. Prack and Y. Matsuda : IEEE Trans. on Components, Hybrids, and Manufacturing Technology, 16 (1993) 919
13. J. Love and P. F. Packman : J. Adhesion, 40 (1993) 139
14. S. M. Song, C. E. Park, H. K. Yun, C. S. Hwang, S. Y. Oh and J. M. Park : J. Adhesion Sci. Technol., 12 (1998) 541

15. J. R. G. Evans and D. E. Packham : J. Adhesion, 9 (1978) 267
16. V. Ashworth and D. Fairhurst : J. Electrochem. Soc., 124 (1977) 506
17. H.-H. Strehblow and B. Titze : Electrochemica Acta, 55 (1980) 839
18. H. Y. Lee and J. Yu : J. of the Korean Inst. of Surf. Eng., 30 (1999) 531
19. T. S. Oh, R. M. Cannon and R. O. Ritchie : J. Am. Ceram. Soc., 70 (1987) C-352
20. Z. Suo and J. W. Hutchinson : Mater. Sci. and Eng., A107 (1989) 135
21. Denny A. Jones : Principles and Prevention of Corrosion, Maxwell Macmillan, (1992) 411
22. M. Cailler and J.-P. Ganachaud : Scanning Microsc. Suppl., J. Schou, P. Kruit, and D. E. Newbury, 4th ed., 57
23. M. Cailler and J.-P. Ganachaud : Scanning Microsc. Suppl., J. Schou, P. Kruit, and D. E. Newbury, 4th ed., 81